NJC

Accepted Manuscript

Journal Name

ARTICLE

Low cost and binder free paper-based cobalt electrode for sodium borohydride electrooxidation

Dongming Zhang, Ke Ye, Jinling Yin, Kui Cheng, Dianxue Cao，Guiling Wang*

A low cost and binder free cobalt electrode is prepared by electrodeposition of Co nano-plates onto a flexible conductive substrate, which is prepared simply by scratching a piece of A4 paper with a common 8B pencil. The morphology and phase structure of the cobalt-graphite-paper (CGP) electrode are characterized by scanning electron microscopy, transmission electron microscope and X-ray diffractometer. The catalytic activity of the CGP electrode for $NaBH_4$ electrooxidation is investigated by means of cyclic voltammetry and chronoamperometry. The catalyst combines tightly with the paper and exhibits a good stability. The oxidation current density reaches to 180 mA cm^{-2} in 1 mol dm^{-3} NaOH and 0.10 mol dm^{-3} $NaBH_4$.

1. Introduction

Driven by the depletion of fossil fuel resources and the ever-increase of environmental pollution, the use of clean energy has become an irreversible trend. In recent years, hydrogen energy exhibits a hopeful application prospect as an environmentally friendly energy carrier due to its high energy density, ease of production from renewable sources and lack of undesirable combustion products [1-5]. The employ of hydrogen as fuel in fuel cells to provide power has been widely studied by scientists [6-8]. However, the commercialization of hydrogen is hampered by the lack of a highly efficient and cost-effective method for the storage of hydrogen. So, the study of hydrogen materials to substitute hydrogen as the hydrogen sources for fuel cells has been a hot topic [9-10].

Nowadays, sodium borohydride ($NaBH_4$), a promising hydrogen storage material with high hydrogen content (10.6 wt. %), high energy density (9.3 Wh g^{-1}), high chemical stability in alkaline solution, non-toxic, and easy handling, has been employed as the anode fuel for direct borohydride fuel cells (DBFCs) and attracted much attention [11-30]. Besides, the complete electrooxidation of $NaBH_4$ generates 8 electrons (Eq.1) [11-30], which is higher than the electrooxidation of hydrogen [6-8], hydrazine [9], methanol [31], ethanol [32], and so on.

In the electrooxidation of $NaBH_4$, the electrode material is clearly an important parameter where a high efficient electro-catalyst is needed. As described previously, precious metal catalysts (Eg. Pt, Pd, Au, Os, Ag) and their alloys [18-23] exhibit high catalytic activity for the electrooxidation of $NaBH_4$. However, the high cost and limited resources restricted their extensive utilization. In the past years, hydrogen storage alloys (Eg. AB_5, AB_2-type alloys) [24-26] and transition metals (Eg. Ni, Cu, Zn, Co) [24, 27-30] are alternative low cost catalysts for $NaBH_4$ electrooxidation but they have lower catalytic activity than precious metals. So preparing the non-precious catalysts with high catalytic activity is significant for the development of low cost and high performance DBFCs. Our team has reported AB_5-type alloy [26], Ni [27], Co [30] electrodes with high catalytic activity for the electrooxidation of $NaBH_4$ previously.

The substrate is one of the decisive factors that determine the applications and performance of the electrode. In general, metal substrates (Eg. Ni foam, Cu foil, Ti foil) [33-35] are widely employed as the electrode collectors due to their electronic conductivity. However, they suffer the drawbacks of limited metal resources, ease of corrosion and high cost. Besides, the employ of binder (Eg. Nafion, polytetrafluoroethene) [18, 26] during the coating process reduces the electronic conductivity of the electrode and decreases the catalytic activity. Recently, preparing electrodes by the ways without scraper smearing, such as electrodeposition and hydrothermal methods, on non-contained metal substrates has become a hot topic. H. N. Alshareef et al. fabricated nanostructured MnO_2 carbon nanotube (CNT) sponge hybrid electrodes as supercapacitors [36]. Y. Cui et al. prepared carbon nanotube (CNT)–textile–Pt cathodes for microbial fuel cell [37]. Out team reported Ni@MWNTs/Sponge [27] and cobalt-multiwalled carbon nanotubes-cosmetic cotton (Co-MWNTs-CC) for $NaBH_4$ electrooxidation [30]. The sponge and textile are cheaper and more stable than the conventional metal electrodes and all of

them achieved high performance. However, the carbon nanotubes are expensive.

$$BH_4^- + 8OH^- \rightarrow BO_2^- + 4H_2O + 8e^- \qquad (1)$$
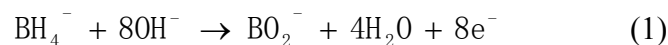
Paper, prepared by vegetable fibre, ash content and some resin, is one of the four great inventions of ancient China and can be found almost anywhere in the world. Nowadays, there has been much interest in the development of electronic and energy storage devices using paper due to its low cost, ease to get, roll-to-roll fabrication, degradability and so on [38-42]. Y Cui et al. invented an Ag modified paper to obtain a 1D flexible electrode substrate for an energy-storage device [38]. K. Chan et al. showed a $Li_4Ti_5O_{12}$/ $LiCoO_2$-CNT/PVDF-paper as the electrode for lithium-ion batteries. Both of the two kinds of electrodes get high electrochemical performances [39]. Besides, all of them are much lighter. However, the Ag and CNT inks are still a bit expensive.

In this paper, we make a conductive paper by conformal coating of graphite with a common 8B pencil on the surface of a piece of A4 paper. Then we employ electrochemical deposition method to prepare three dimensional (3D) cobalt nanoplates on the one dimensional (1D) conductive paper. The binder-free Co-graphite-paper (CGP) electrode exhibits a high catalytic activity for the electrooxidation of $NaBH_4$ due to its large specific area and high electronic conductivity.

2. Experimental

All chemicals were analytical grade and were used without further purification. The A4 paper (70 g m^{-2}, Shenyang Jinxin office equitment Co. Ltd.) is commercially availiable printing paper, which is made up of vegetable fibres (EG. Cellulose, hemicellulose, lignin) and some calcium salts (EG. $CaCO_3$, $CaSO_4$). A common 8B pencil (Shanghai Yinzun company) was used to draw on the A4 paper uniformly for two times and form a conductive graphite/paper current collector. The resistance of the GP substrate is about 20 Ω/square, measured by four points probe technique. The as-prepared graphite/paper collector was cut into 1×1 cm^2 and then immersed in 2.5 mol dm^{-3} KCl, 0.4 mol dm^{-3} NH_4Cl, 0.5 mol dm^{-3} H_3BO_3 and 1.0 mol dm^{-3} $CoCl_2\cdot6H_2O$ for the electrodeposition of Co film on the graphite/paper substrate, which was performed using the Autolab PGSTAT302 (Eco Chemie) electrochemical workstation in a conventional three electrode electrochemical cell with a saturated Ag/AgCl, KCl reference electrode and Pt foil counter electrode. The KCl serves as supporting electrolyte and improves the conductivity of the solution. The NH_4Cl and H_3BO_3 serve as substances to adjust the PH of electrodeposition electrolyte to 4.6. The graphite is hydrophobic and the surface of the GP substrate is a hydrophobic surface. In order to ensure the Co can be electrodeposited to the surface of GP substrate successfully, the electrolyte solution must contact with the GP closely. The carbon element contained in graphite will be oxidized to COO- at high potential. So, first was a 20 min 1.0 V oxidation potential which made the graphite surface transform

into a hydrophilic surface. Then the electrodeposition was carried out at a constant potential of -0.8 V for 150 min to form the Co-graphite-paper film (CGP) electrode [43]. The clathrate of $Co(H_2O)_6^{2+}$ is the predominant solution species in acidic electrolyte. These transients present the characteristic features of a nucleation process with three-dimensional growth of nuclei limited by the diffusion of the electroactive species. At the fixed electrodeposition potential, the formation of 3D islands was observed giving rise to perpendicular magnetisations to form Co 3D structure [43-45]. The mass of the Co on the paper is about 8 mg cm^{-2}.

$NaBH_4$ electrooxidation was also performed in the same three-electrode electrochemical cell using the 1 cm^2 CGP electrode. All potentials were referred to the saturated Ag/AgCl, KCl reference electrode. The morphology of the electrodes was determined using a scanning electron microscope (SEM, JEOL JSM-6480) and transmission electron microscope (TEM, FEI TeccaiG2S-Twin, Philips). The structure was analyzed by a powder X-ray diffractometer (XRD, Rigaku TTR-III) equipped with Cu Kαradiation (λ= 0.15406 nm).

3. Results and discussions

Fig. 1 shows the fabrication process of the Co-Graphite-Paper (CGP) electrode. First, a graphite layer is constructed on the paper after a conventional painting process. The graphite layer exhibits a good ductility and electronic conductivity for the electrodeposition of Co. Besides, the graphite conglutinates tightly on the surface of the paper and ensures a high stability for the electrode. Second, the hydrophilic –COOH occurs on the graphite surface, which is favourable for the electrodeposition of Co. At last, the metallic Co film comes into being at a constant potential.
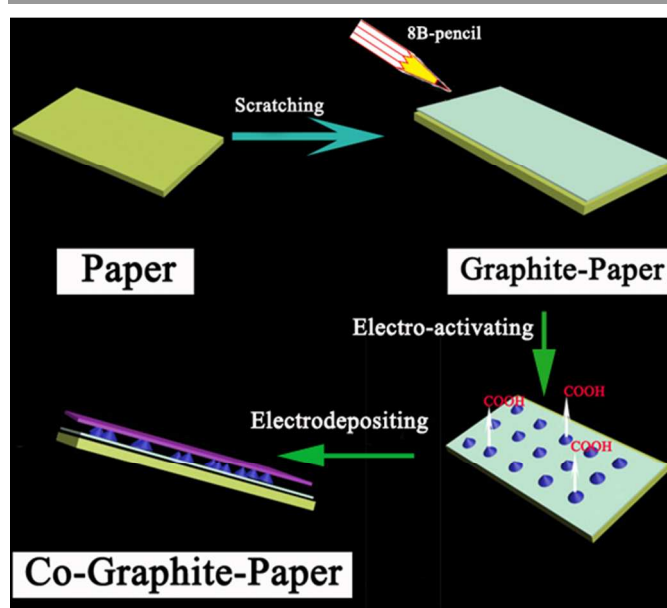

Fig. 1 The fabrication process of the Co-Graphite-Paper (CGP) electrode.

Fig. 2 shows the SEM images of graphite-paper (GP) substrate (Fig. 2a) and CGP electrode (Fig. 2b-c) and TEM image of Co nano-plate (Fig. 2d). Fig. 2a exhibits a flat graphite layer. The graphite layer leads to a 1D electronic conductive layer and acts as a transition layer for the electrodeposition of Co. Besides, the preparation of the graphite layer does not use any binder, which ensures a high conductivity and stability of the CGP electrode. Fig. 2b shows a film-like Co layer. It is obvious that the Co distributes uniformly on the surface of the GP substrate at low magnification. Compared with the Co film in Fig. 2b, Fig. 2c shows the microstructure of the Co film at high magnification. Clearly, the metallic Co exhibits a nano-plates structure. The diameters of the Co nano-plates are around 500 nm and they own a higher specific area than the normal planar electrode (EG. Al foil, Cu foil). Besides, these Co nano-plates distribute intricately, which is benefit for the diffusion of the $NaBH_4$ and will lead to a high catalytic performance. Insert in Fig. 2c is the corresponding elemental distributions of carbon and cobalt. First, it is obvious that the carbon element distributes among the interval of the Co nanoplates, which implies that the fuel can diffuse into these intervals and be fully exploited during the test process. Besides, it is clear that the electrode is fully covered by Co element, which demonstrates that the Co nanoplates uniformly scatter on the electrode surface. Fig. 2d shows the TEM of the single Co nano-plate. As can be seen, the width of the Co nano-plate is about 500 nm, which is in accord with the SEM image. The edge of the Co nano-plate is not smooth but rough, which will provide a high surface energy for the $NaBH_4$ electrooxidation reaction [27].
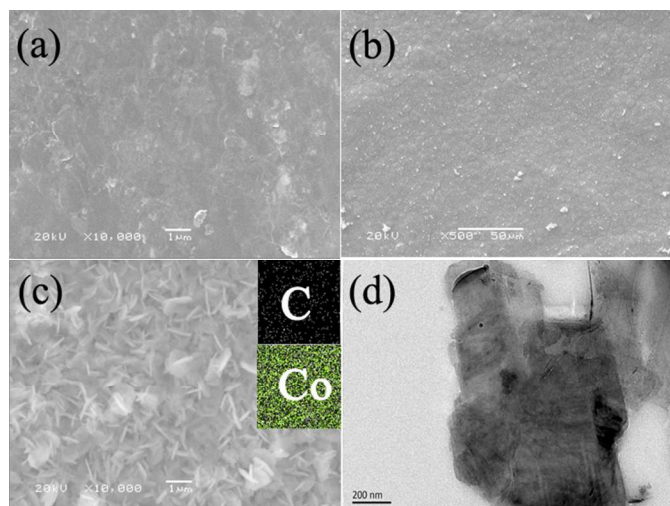

Fig. 2 the SEM images of graphite-paper (GP) substrate (Fig. 2a) and Co-graphite-paper (CGP) electrode (Fig. 2b-c) and TEM image of Co nano-plate (Fig. 2d); Insert in c is the corresponding elemental distribution of carbon and cobalt.

Fig. 3 shows the XRD patterns of the graphite-paper (GP) substrate and Co-graphite-paper (CGP) electrode. As can be seen from GP curve, seven strong diffraction peaks are located during 30° to 60 ° and many weak diffraction peaks are throughout of the whole scanning scope, all of which can be attributed to the main ingredients of the A4 paper and graphite

(Eg. $CaCO_3$, $CaSO_4$, cellulose, carbon). Compared with the GP curve, there are five palpable diffraction peaks at 2θ values of 41.7°, 44.2°, 47.5°, 51.5° and 75.9° and all of these peaks can be indexed to (1 0 0), (0 0 2), (1 0 1), (2 0 0) and (1 1 0) plane reflections of the metallic Co (JCPDS Card NO. 05-0727).
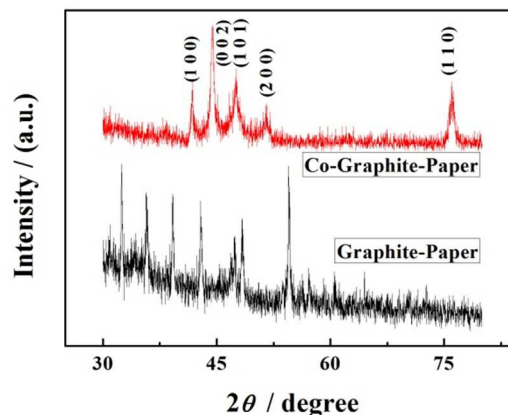

Fig. 3 The XRD patterns of the GP substrate and CGP electrode.

Fig. 4 shows the cyclic voltammograms (CVs) of the GP substrate and CGP electrode in 1 mol dm^{-3} NaOH with (Fig. 4a) and without (Fig. 4b) 0.1 mol dm^{-3} $NaBH_4$. Fig. 4a shows that the GP substrate is almost no activity in bare alkaline electrolyte. However, the oxidation current density reaches to 18 mA cm^{-2} at -0.78 V on the CGP electrode, which implies that the CGP electrode own a much higher catalytic activity than the GP substrate. Besides, the obvious oxidation peak at around -0.78 V in the positive scan on the CGP can be attributed to the reaction of metallic Co to $Co(OH)_2$ according to the previous reports [46]. Fig. 4b shows that the CGP electrode exhibits a much higher catalytic activity than the GP substrate for $NaBH_4$ electrooxidation, which is consistent with Fig. 4a. The open circuit potential (OCP) at CGP electrode is around -1.20 V due to the electrooxidation of hydrogen (Eq. 3) [20, 28] released from the hydrolysis of $NaBH_4$ (Eq. 2) [11-30] and the incomplete electrooxidation of $NaBH_4$ (Eq. 4) [20]. The CGP electrode exhibits two obvious oxidation peaks at about -0.7 V and -0.4 V, which can be attributed to the electrooxidation of hydrogen (Eq. 3) [20, 28, 30] and BH_4^- (Eq. 1) [11-30], respectively. However, there is no corresponding reduction peak at the negative scan, which demonstrates that both of the electrooxidation of hydrogen and BH_4^- are irreversible. Besides, it is clear that the oxidation current density reaches to 140 and 180 mA cm^{-2} at -0.7 V and -0.4 V, respectively, which proves that the number of electrons released by the direct electrooxidation of BH_4^- is more than that by the electrooxidation of hydrogen at the CGP electrode. In consideration of the mass of the Co, the oxidation current density reaches to 22.5 mA $(cm^2\ mg)^{-1}$ in 0.10 mol dm^{-3} BH_4^- at -0.4 V, which is much higher than the reported Ni powders 1.2 mA $(cm^2\ mg)^{-1}$ [24] in 0.90 mol dm^{-3} BH_4^- at -0.6 V, $LaNi_{4.5}Al_{0.5}$-Au 0.75 mA $(cm^2\ mg)^{-1}$ [25] in 1.00 mol dm^{-3} BH_4^-

at -0.4 V, Ni@MWNTs/Sponge 22.35 mA (cm^2 mg)$^{-1}$ [27] in 0.1 mol dm^{-3} BH$_4^-$ at -0.6 V and Co-MWNTs-CC 18.83 mA (cm^2 mg)$^{-1}$ [30] in 0.1 mol dm^{-3} BH$_4^-$ at -0.6 V. The high catalytic activity of the CGP electrode can be attributed that large surface area of Co and the unique 3D structure of the electrode, which benefit the diffusion of BH$_4^-$ and OH$^-$ to the surface catalytic active sites and remarkably lower the concentration polarization. Besides, the non-binder in whole preparation process may be an important reason, which is leading to that the CGP electrode shows much more superior catalytic performance than the directly coated electrode [24-25].
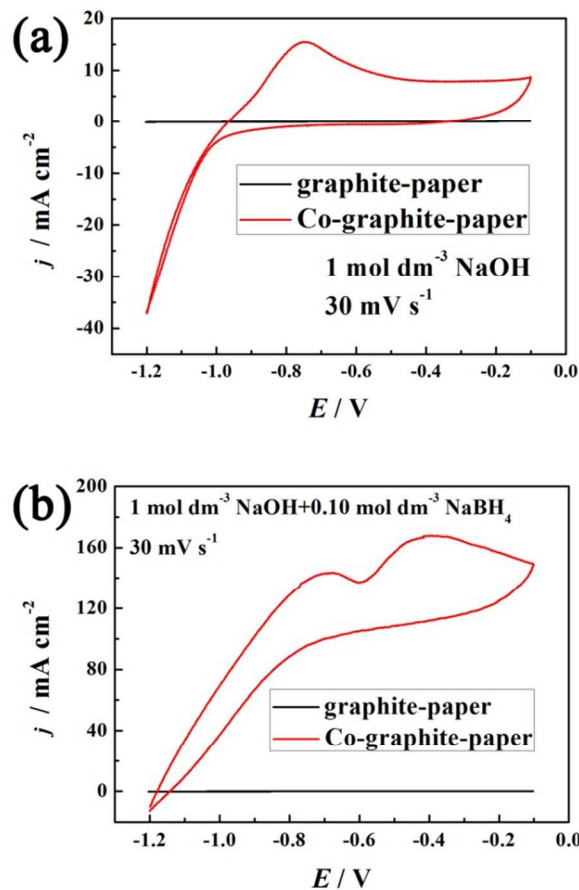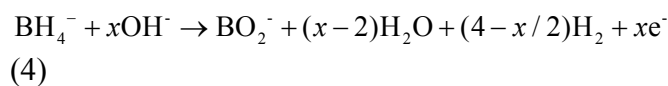

Fig. 4 The cyclic voltammograms (CVs) of the GP substrate and CGP electrode in 1 mol dm^{-3} NaOH without (Fig. 4a) and with (Fig. 4b) 0.1 mol dm^{-3} NaBH$_4$.

$$BH_4^- + 2H_2O \rightarrow BO_2^- + 4H_2 \qquad (2)$$

$$H_2 + 2OH^- \rightarrow 2H_2O + 2e^- \qquad (3)$$

$$BH_4^- + xOH^- \rightarrow BO_2^- + (x-2)H_2O + (4-x/2)H_2 + xe^- \qquad (4)$$

The effects of NaOH concentration on NaBH$_4$ electrooxidation at CGP electrode is given in Fig. 5. NaOH not only serves as supporting electrolyte, but also participate in the NaBH$_4$

electrooxidation (Eq. 1 and 4) [11-30]. The concentration of NaBH$_4$ is fixed at 0.10 mol dm^{-3} and the concentration of NaOH varies from 1 to 4 mol dm^{-3}. All of the open circuit potentials (OCP) are around -1.2 V, which demonstrates that the OCP of the NaBH$_4$ electrooxidation is independent of the NaOH concentration. However, it is obvious that both of the potentials of electrooxidation peaks of the hydrogen and BH$_4^-$ move more positive. Besides, both of the electrooxidation current density of the electrooxidation of hydrogen and BH$_4^-$ decrease with increasing the NaOH concentration. A large amount of BH$_4^-$ diffuses to the CGP electrode surface and oxidized to release electrons, when the NaOH concentration is low. However, compared with the low NaOH concentration, the flux ratio of [OH$^-$/BH$_4^-$] increased and the amount of BH$_4^-$ diffused to the electrode surface decreases, which will lead a more serious concentration polarization and low the electrooxidation behaviour of NaBH$_4$ on the electrode surface and then lead a low catalytic performance at high NaOH concentration. Besides, the more OH$^-$ may occupy the CGP electrode surface, which will decrease the contact chance between BH$_4^-$ and Co-catalyst and then reduce the performance of NaBH$_4$ electrooxidation.
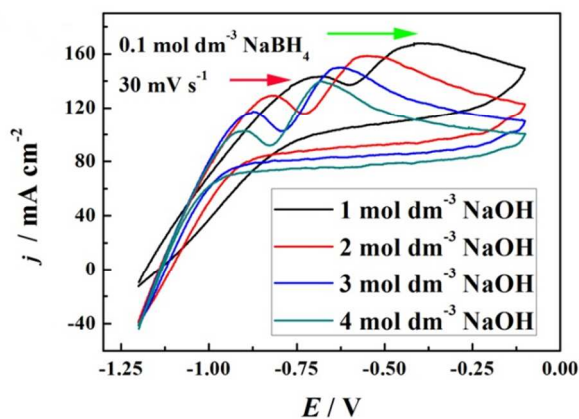

Fig. 5 CVs of CGP in 0.10 mol dm^{-3} NaBH$_4$ and x mol dm^{-3} NaOH (x=1, 2, 3, 4)

Fig. 6 shows the effects of NaBH$_4$ concentration on the NaBH$_4$ electrooxidation at the CGP electrode. The NaOH concentration is fixed at 1 mol dm^{-3} and the concentration of NaBH$_4$ varies from 0.05 to 0.20 mol dm^{-3}. At low NaBH$_4$ concentrations (0.05-0.15 mol dm^{-3}), both of the electrooxidation peaks of hydrogen and BH$_4^-$ are obvious. The oxidation current density increases from 75 to 210 mA cm^{-2} correspond to the electrooxidation of hydrogen with increasing the NaBH$_4$ concentration from 0.05 to 0.15 mol dm^{-3}. The result is caused by the increased volume of hydrogen according to the Eq. 2 and 3. At the same time, the current density increases from 115 to 220 mA cm^{-2} correspond to the direct electrooxidation of BH$_4^-$ (Eq. 1). However, both of the two oxidation peaks disappear when the NaBH$_4$ concentration increases to 0.20 mol dm^{-3}, which demonstrates that both of the electrooxidation of hydrogen and BH$_4^-$ are controlled by diffusion at low NaBH$_4$

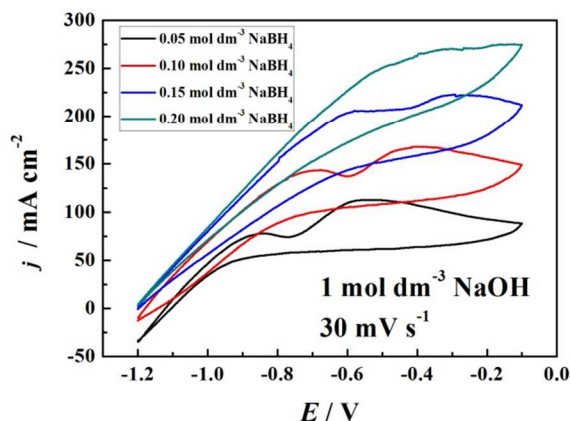concentration and electrochemical polarization at high NaBH$_4$ concentration.

Fig. 6 CVs of CGP electrode in 1 mol dm-3 NaOH and x mol dm-3 NaBH4 (x=0.05, 0.10, 0.15, 0.20)

Fig. 7a shows the CVs of NaBH$_4$ electrooxidation at the CGP electrode recorded at different scan rate in a solution containing 4 mol dm^{-3} NaOH and 0.10 mol dm^{-3} NaBH$_4$. All of the potentials of the hydrogen electrooxidation peaks are located at around -0.8 V, demonstrating that the reaction rate of the hydrogen electrooxidation is fast and controlled by electrochemical reaction when the NaBH$_4$ concentration is fixed. As a contrast, the BH$_4^-$ electrooxidation peak potential gets more positive and the plot of Ip as a function of the $v^{1/2}$ exists linear relationship with increasing the scan rate, which indicated that the reaction rate of the BH$_4^-$ electrooxidation is lower than the electrooxidation of hydrogen.
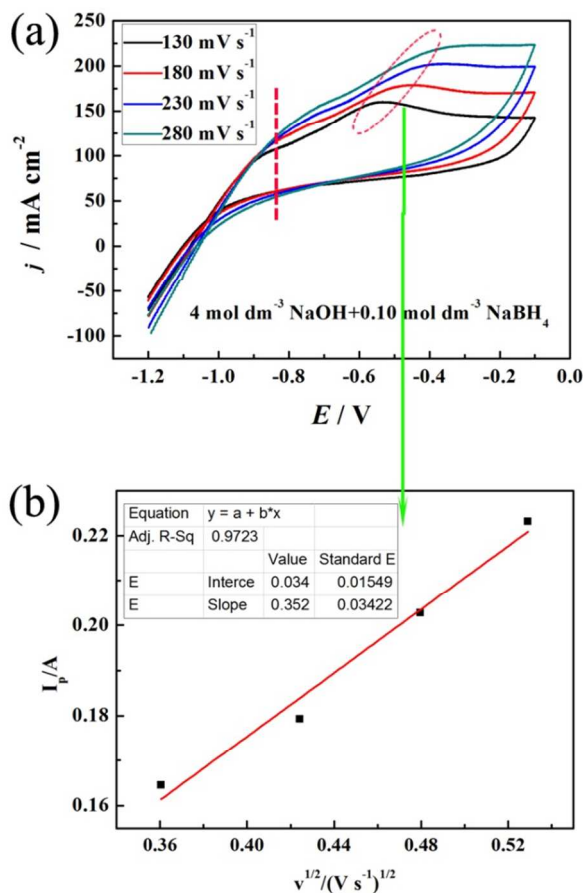

Fig. 7 CVs of NaBH$_4$ electrooxidation at the CGP electrode in 4 mol dm^{-3} NaOH and 0.10 mol dm^{-3} NaBH$_4$ at different scan rates (130-280 mV s^{-1}) (a); the plot of Ip vs. $v^{1/2}$ (b).

Fig. 8 shows the chronoamperometric curves (CAs) of different potentials in 4 mol dm^{-3} NaOH and 0.10 mol dm^{-3} NaBH$_4$ at CGP. The current-time curves are quite stable during the reaction process at -1.1 V, which may be attributed to the constant surface of the electrode and the unfallen activity substance. However, at -0.3 V, the rate of electrochemical reaction is much higher than it at -1.1 V, which consumes more fuel (NaBH$_4$) during the long time test. So the chronoamperometric curve declines in the reaction process at -0.3 V. It is clear that the current density at -0.3 V is higher than it at -1.1 V, which demonstrates that the electrooxidation of BH$_4^-$ releases more electrons than the electrooxidation of hydrogen. The result is consistent with the CVs.
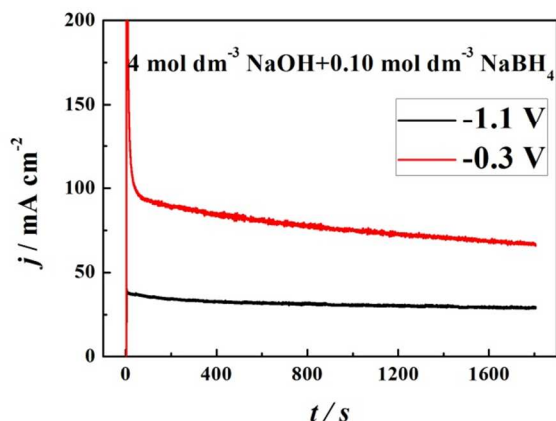
Fig. 8 Chronoamperometric curves (CAs) for $NaBH_4$ electrooxidation at different potentials (-1.1 and -0.3 V) in 4 mol dm^{-3} NaOH and 0.10 mol dm^{-3} $NaBH_4$.

4. Conclusions

In this paper, a graphite-paper (GP) substrate is prepared by coating a layer of graphite onto a piece of A4 paper with an ordinary 8B pencil. Then a cobalt-graphite-paper (CGP) electrode is fabricated by electrodepositing a three dimensional (3D) nano-structure Co film onto the 1D-GP substrate. The electrode exhibited high electrocatalytic activity and superior stability for $NaBH_4$ electrooxidation in a NaOH solution. The high performance is ascribed to the 3D nano structure. In association with the delightful electrochemical performance, low-cost and lightweight, CGP is undoubtedly emerging as promising renewable anode material for DBFCs in future.

Acknowledgments

Notes and references

Key Laboratory of Superlight Materials and Surface Technology of Ministry of Education, College of Materials Science and Chemical Engineering. Harbin Engineering University, Harbin, 150001, P.R.China. E-mail: wangguiling@hrbeu.edu.cn; Fax: +010-86-451-82589036; Tel: +010-86-451-82589036

Electronic Supplementary Information (ESI) available: S1. $NaBH_4$ electrooxidation activities on the CGP electrodes prepared with different electrodeposition time (50, 100, 150, 200 min) in 1 mol dm^{-3} NaOH and 0.1 mol dm^{-3} $NaBH_4$; S2. The electrode stability test in highly alkaline medium.

1. A. Midilli, M. Ay, I. Dincer and M. A. Rosen, Renew. Sustain. Energy Rev., 2005, 9, 255-271.
2. L. Barreto, A. Makihira and K. Riahi, Int. J. Hydrogen Energy, 2003, 28, 267-284.
3. I. Dincer, Renew. Sustain. Energy Rev., 2000, 4, 157-175.
4. T. M. Nenoff, M. R. Berman, K. C. Glasgow, M. C. Cesa and H. Taft, Ind. Eng. Chem. Res., 2012, 51, 11819-11820.
5. A. Haryanto, S. Fernando, N. Murali and S. Adhikari, Energy Fuels, 2005, 19, 2098-2106.
6. S.-B. Han, Y.-J. Song, Y.-W. Lee, A. R. Ko, J.-K. Oh and K.-W. Park, Chem. Commun., 2011, 47, 3496-3498.
7. H. A. Gasteiger, N. M. Markovic and P. N. Ross, J. Phys. Chem., 1995, 99, 8290-8301.
8. A. N. Simonov, P. E. Plyusnin, Y. V. Shubin, R. I. Kvon, S. V. Korenev and V. N. Parmon, Electrochim. Acta, 2012, 76, 344-353.
9. G. E. Evans and K. V. Kordesch, Science, 1967, 158, 1148-1152.
10. X.-B. Zhang, S. Han, J.-M. Yan, H. Shioyama, N. Kuriyama, T. Kobayashi and Q. Xu, Int. J. Hydrogen Energy, 2009, 34, 174-179.
11. G. Rostamikia and M. J. Janik, Energy Environ. Sci., 2010, 3, 1262-1274.
12. J. Ma, N. A. Choudhury and Y. Sahai, Renew. Sustain. Energy Rev., 2010, 14, 183-199.
13. B. H. Liu and Z. P. Li, J. Power Sources, 2009, 187, 291-297.
14. D. M. F. Santos and C. A. C. Sequeira, Renew. Sustain. Energy Rev., 2011, 15, 3980-4001.
15. G. H. Miley, N. Luo, J. Mather, R. Burton, G. Hawkins, L. Gu, E. Byrd, R. Gimlin, P. J. Shrestha, G. Benavides, J. Laystrom and D. Carroll, J. Power Sources, 2007, 165, 509-516.
16. N. A. Choudhury, J. Ma and Y. Sahai, J. Power Sources, 2012, 210, 358-365.
17. D. M. F. Santos, P. G. Saturnino, R. F. M. Lobo and C. A. C. Sequeira, J. Power Sources, 2012, 208, 131-137.
18. L. Yi, L. Liu, X. Liu, X. Wang, W. Yi, P. He and X. Wang, Int. J. Hydrogen Energy, 2012, 37, 12650-12658.
19. K. Cheng, D. Cao, F. Yang, L. Zhang, Y. Xu and G. Wang, J. Mater. Chem., 2012, 22, 850-855.
20. P. He, X. Wang, Y. Liu, X. Liu and L. Yi, Int. J. Hydrogen Energy, 2012, 37, 11984-11993.
21. D. M. F. Santos and C. A. C. Sequeira, Electrochim. Acta, 2010, 55, 6775-6781.
22. M. H. Atwan, D. O. Northwood and E. L. Gyenge, Int. J. Hydrogen Energy, 2005, 30, 1323-1331.
23. E. Sanlı, H. Çelikkan, B. Zühtü Uysal and M. L. Aksu, Int. J. Hydrogen Energy, 2006, 31, 1920-1924.
24. B. H. Liu and S. Suda, J. Alloys Compd., 2008, 454, 280-285.
25. Z. Yang, L. Wang, Y. Gao, X. Mao and C.-A. Ma, J. Power Sources, 2008, 184, 260-264.
26. D. Zhang, G. Wang, K. Cheng, J. Huang, P. Yan and D. Cao, J. Power Sources, 2014, 245, 482-486.
27. D. Zhang, K. Cheng, N. Shi, F. Guo, G. Wang and D. Cao, Electrochem. Commun., 2013, 35, 128-130.
28. D. Duan, Y. Zhao, S. Liu, and A. Wu, Adv. Mater. Res., 2012, 347-353, 3264-3267.
29. D. M. F. Santos and C. A. C. Sequeira, J. Electrochem. Soc., 2010, 157, B13-B19.
30. D. Zhang, K. Ye, K. Cheng, D. Cao, J. Yin, Y. Xu, G. Wang, Int. J. Hydrogen Energy, 2014, 39, 9651-9657.
31. Y. Zhang, M. Janyasupab, C.-W. Liu, X. Li, J. Xu and C.-C. Liu, Adv. Funct. Mater., 2012, 22, 3570-3575.

32. C. W. Xu, H. Wang, P. K. Shen and S. P. Jiang, Adv. Mater., 2007, 19, 4256-4259.

33. J. Wei, G. Xing, L. Gao, H. Suo, X. He, C. Zhao, S. Li and S. Xing, New J. Chem., 2013, 37, 337-341.

34. X. Dong, K. Wang, C. Zhao, X. Qian, S. Chen, Z. Li, H. Liu and S. Dou, J. Alloys Compd., 2014, 586, 745-753.

35. Y. Song, S. Qin, Y. Zhang, W. Gao and J. Liu, J. Phys. Chem. C, 2010, 114, 21158-21164.

36. W. Chen, R. B. Rakhi, L. Hu, X. Xie, Y. Cui and H. N. Alshareef, Nano Lett., 2011, 11, 5165-5172.

37. X. Xie, M. Pasta, L. Hu, Y. Yang, J. McDonough, J. Cha, C. S. Criddle and Y. Cui, Energy Environ. Sci., 2011, 4, 1293-1297.

38. L. Hu, J. W. Choi, Y. Yang, S. Jeong, F. La Mantia, L.-F. Cui and Y. Cui, Proc. Natl Acad. Sci., 2009, 106, 21490-21494.

39. Q. Cheng, Z. Song, T. Ma, B. B. Smith, R. Tang, H. Yu, H. Jiang and C. K. Chan, Nano Lett., 2013, 13, 4969-4974.

40. T. H. Nguyen, A. Fraiwan and S. Choi, Biosens. Bioelectron., 2014, 54, 640-649.

41. N. Ruecha, R. Rangkupan, N. Rodthongkum and O. Chailapakul, Biosens. Bioelectron., 2014, 52, 13-19.

42. L. Nyholm, G. Nyström, A. Mihranyan and M. Strømme, Adv. Mater., 2011, 23, 3751-3769.

43. Z.F. Lodhi, J.M.C. Mol, W.J. Hamer, H.A. Terryn, J.H.W. De Wit, Electrochim. Acta,, 2007, 52, 5444-5452.

44. M. Palomar-Pardavé, I. González, A.B. Soto, E.M. Arce, J. Electroanal. Chem., 1998, 443, 125-136.

45. S. Floate, M. Hyde, R.G. Compton, J. Electroanal. Chem., 2002, 523, 49-63

46. J. Liu, R. Liu, C. L. Yuan, X. P. Wei, J. L. Yin, G. L. Wang and D. X. Cao, Fuel Cells, 2013, 13, 903-909..
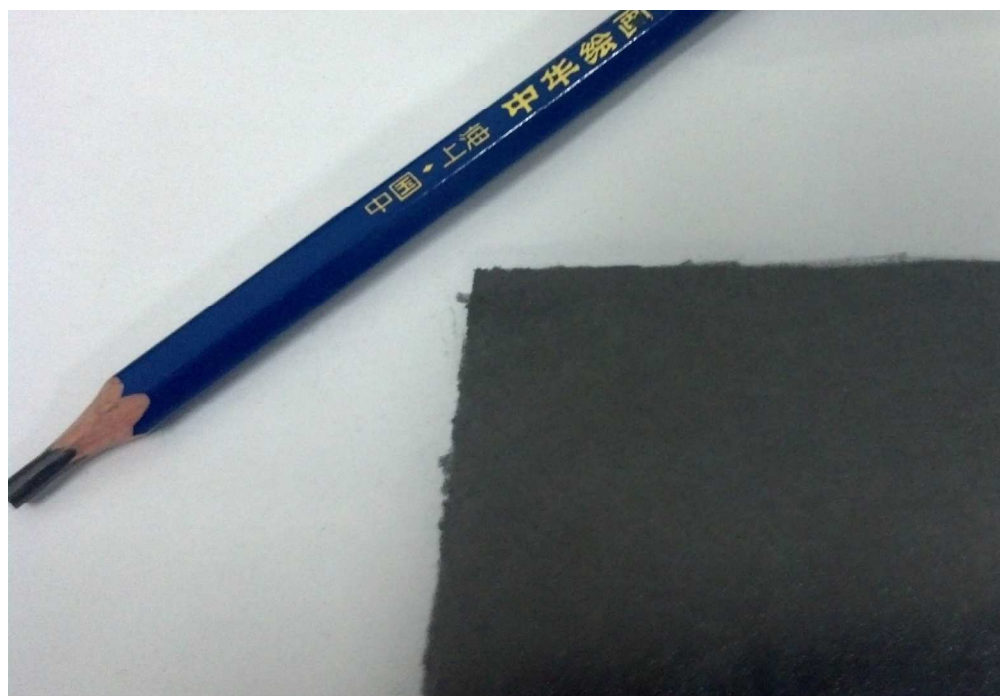
Abstract-picture
886x611mm (72 x 72 DPI)